Cell. Mol. Biol. (ISSN: 1165-158X)

Journal Homepage: www.cellmolbiol.org

Cellular and Molecular Biology

Original Article

Harnessing natural compounds for PIM-1 kinase inhibition: A synergistic approach using virtual screening, molecular dynamics simulations, and free energy calculations

Qazi Mohammad Sajid Jamal*

Department of Health Informatics, College of Applied Medical Sciences, Qassim University, Buraydah 51452, Saudi Arabia

Article Info

Article history:

Received: September 15, 2024
Accepted: October 06, 2024
Published: November 30, 2024

Use your device to scan and read the article online

Abstract

Cancer has substantial economic ramifications for healthcare systems. PIM kinases, specifically PIM-1, are commonly upregulated in different types of cancers, thereby promoting cancer development. PIM-1 inhibitors have garnered interest for their potential efficacy in cancer therapy. This study used computational methods to screen a library of 7,600 natural compounds aimed at the PIM-1 active site. Top five candidates ZINC00388658, ZINC00316459, ZINC00197401, ZINC00001673, and ZINC00316479 were identified in the study. These compounds were further evaluated through molecular dynamics simulations (MDS) and free energy calculations using the MMPBSA method. These compounds interacted with key PIM-1 residues and had multiple common binding site interactions with the co-crystallized ligand 6YN, which was used as a control. Furthermore, the selected compounds exhibited favorable drug-like properties and stable docked complexes during a 200-ns molecular dynamics simulation, followed by MMPBSA analysis. Among the candidates, ZINC00388658 had the most favorable binding energy profile, indicating exceptional stability and intense interaction with PIM-1. This makes ZINC00388658 the most promising candidate for further development as a PIM-1 inhibitor. These findings suggest that ZINC00388658 and other promising compounds hold significant potential for developing new cancer therapies that target PIM-1.

Keywords: Cancer; PIM-1; Molecular dynamics simulation; MMPBSA, Natural compounds; Virtual screening

1. Introduction

Cancer is a prevalent disease that has a significant financial impact on healthcare. It is characterized by aberrant cell proliferation brought on by genetic mutations, leading to the development of malignant tumors [1]. Cancer is one of the top two causes of death before the age of 70 in 112 of 183 countries [2]. According to projections, there were 1,958,310 new cancer cases and 609,820 cancer-related deaths in the United States in 2023. Notably, the incidence of prostate cancer increased by 3% on an annualized basis from 2014 to 2019, reversing a two-decade decline. This change resulted in an additional 99,000 new cases; otherwise, male incidence trends were more favorable than female incidence trends [3]. Cancer treatment has been transformed by the development of targeted therapies [4].

The Moloney murine leukemia (PIM) kinases are a subset of serine/threonine kinases that include three isoforms: PIM-1, PIM-2, and PIM-3. These kinases have been shown to be important in enhancing hematopoietic cell proliferation in response to growth factors and cytokines [5, 6]. Notably, abnormally elevated PIM kinase levels have been linked to the onset of cancer in transgenic animal models [7] and play a multifaceted role in carcinogenesis, including activities such as multiple myeloma proliferation promotion, facilitation of anti-apoptotic processes, cell cycle modulation, and bone destruction mediation [8, 9]. PIM-1 overexpression has been observed in various cancers [10-14]. Notably, the absence of apparent abnormalities in PIM-1 kinase-deficient animals emphasizes its suitability as a prime target for developing novel anticancer therapeutics [15]. Furthermore, PIM-1 contributes to drug resistance mediation by phosphorylating and stabilizing drug efflux transporters such as P-glycoprotein and breast cancer resistance protein [16, 17], emphasizing the critical need for the development of effective PIM-1 inhibitors.

The implications of PIM kinases in key cancer-related processes have spurred vigorous exploration for small molecule inhibitors that act via ATP competition to develop novel targeted therapies for oncological conditions. Despite their commendable biochemical efficacy, most PIM-1 inhibitors have fallen short of becoming clinically relevant anticancer agents owing to suboptimal pharmacological properties [18-20]. PIM-1 inhibitors have sparked considerable interest in recent years, owing primarily to

* Corresponding author.
E-mail address: m.quazi@qu.edu.sa (Q. M. S. Jamal).
Doi: http://dx.doi.org/10.14715/cmb/2024.70.11.22

their therapeutic potential in the context of cancer. The rate of discovery of novel PIM inhibitors has increased noticeably, highlighting the critical need for a new generation of potent compounds with the necessary pharmacological profiles, which have the potential to pave the way for the development of PIM kinase inhibitors effective against cancers.

In silico methodologies have become essential in pharmacological discovery, facilitating the accurate identification and targeting of therapeutic proteins. These methods facilitate the efficient evaluation of natural compounds as prospective inhibitors, offering a more rapid and economical alternative to conventional experimental approaches. Multiple studies have evidenced the efficacy of in silico tools in forecasting interactions between natural compounds and drug targets, thereby considerably enhancing the development of novel therapeutics [21, 22]. This study aimed to employ computational approaches, including molecular docking-based virtual screening (VS) and molecular dynamics approaches, to discover novel natural PIM-1 inhibitors.

2. Methodology

2.1. D Structural assessment of PIM-1

The PIM-1 structural configuration (3D) was obtained from the Protein Data Bank (PDB ID: 5KZI). The X-ray structure of PIM-1 (resolution: 2.10 Å) was complex with an imidazopyridine inhibitor [23]. The heteroatom (imidazopyridine inhibitor) and water molecules were removed using Discovery Studio Visualizer 2020. The Chimera software suite minimized the structure, which began with 100 steps of steepest descent minimization and then 10 steps of conjugate gradient minimization. The prepared protein structure was saved as .pdb for VS.

2.2. Natural compound retrieval and library preparation

Natural compounds were obtained from the ZINC database. Compounds adhering to Lipinski's Rule of Five and molecular weights ranging from 250 to 350 Da were chosen to ensure drug-likeness, as most small-molecule drugs fall between 250 and 500 Da. A total of 7,600 compounds were downloaded in the .sdf format. These compounds were prepared with PyRx 0.8 software, which utilized the Universal Force Field for energy minimization. The energy-minimized compounds were then converted to .pdbqt format for further molecular docking-based VS. The XYZ coordinates for the binding site of PIM-1 were determined using Discovery Studio Visualizer 2020, with values of -41.267870 for the x-coordinate, -2.006370 for the y-coordinate, and 2.111056 for the z-coordinate. The radius was set as 7.253168.

2.3. Structured-based virtual screening

Virtual Screening (VS) is a valuable tool for enhancing the number of active compounds within databases while efficiently filtering out inactive entities prior to empirical validation in laboratory settings. By employing structure-based virtual screening, researchers can focus on compounds that are more likely to interact effectively with specific biological targets [24]. It analyzes large databases of known 3D structures using computer methodologies [25]. The prepared compound library was screened against the PIM-1 active site using the PyRx 0.8 program [26].

1.1. In silico Pharmacokinetics and toxicity estimation

The top five hit compounds obtained through VS were analyzed for their ADMET (absorption, distribution, metabolism, excretion, and toxicity) properties and physicochemical characteristics using the ADMET-AI web interface (https://admet.ai.greenstonebio.com/). . The machine learning tool ADMET-AI utilized predictive algorithms to determine ADMET properties and crucial physicochemical characteristics. The predictions encompassed gastrointestinal absorption, blood-brain barrier permeability, CYP450 interactions, half-life, clearance, and toxicity profiles such as hepatotoxicity and cardiotoxicity. The findings were utilized to assess the drug-like properties and safety of the compounds in anticipation of subsequent investigations [27].

1.2. Molecular dynamics (MD) simulation

The top five selected compounds (ZINC00388658, ZINC00316459, ZINC00197401, ZINC00001673, and ZINC00316479), as well as a control compound, were subjected to MDS with GROMACS 2019.6 software [28] and the CHARMM27 force field [29]and SwissParam [30] was used to generate tology files. The 'particle-mesh Ewald' technique was used to precisely calculate the long-range electrostatic interactions between PIM-1 and the selected compounds. The steepest descent method was used to minimize energy in the system for 1,500 steps. The system then went through two stages of equilibration, first with the NVT ensemble and then with the NPT ensemble. The final manufacturing process was carried out for 200 ns at a constant temperature of 300 Kelvin.

Following the simulation, several analyses were performed using GROMACS analysis tools, including RMSD, RMSF, RoG, H-bond, eigenvector index, and PCA. The 3D models were created using Visual Molecular Dynamics to create graphical representations. These procedures followed protocols as described in earlier studies [31-33].

2.6. MM-PBSA analysis

The Molecular Mechanics-Poisson–Boltzmann Surface Area (MM-PBSA) method [34] based free energy calculation was simulated by MMP-BSA.py Python script [35]. The free energy calculation was performed by gmx_MMPBSA program [36]. The calculation of free energy (ΔG_{bind}) was accomplished by the following formula:

Where;

$\Delta G_{bind} = \Delta EMM + \Delta G_{sol} - T\Delta S$

ΔEMM = Molecular Mechanics energy (van der Waals and electrostatic)

ΔG_{sol} = Solvation free energy (polar and non-polar contributions)

$T\Delta S$ = Entropic contribution

3. Results

This study attempts to identify novel substances that could aid in developing effective cancer treatments by specifically targeting PIM-1, a protein involved in cancer cell survival, growth, and drug resistance. Compounds with molecular weights ranging from 250 to 350 Da were obtained from the ZINC database. 7,600 compounds were retrieved and processed for VS against the binding pocket of PIM-1 kinase. The cocrystal ligand 6YN (PubChem ID: 70984064) was employed as a positive control to compare

Table 1. Top 10 hits and their binding affinity values.

Top 10 hits	Binding affinity (kcal/mol)	Mol. Wt	Smile ID
ZINC00388658	-9.8	298.338	O=C1OC[C@H](Cc2cccc(O)c2)[C@H]1Cc1cccc(O)c1
ZINC00316459	-9.7	283.283	O=C(/C=C/c1ccco1)C[C@@]1(O)C(=O)Nc2ccccc21
ZINC00197401	-9.6	262.309	CC(C)CCOc1ccc([C@H]2NC(=O)NC2=O)cc1
ZINC00001673	-9.5	305.205	N[C@@H](Cc1ccc(N(CCCl)CCCl)cc1)C(=O)O
ZINC00316479	-9.4	335.315	O=C(C[C@@]1(O)C(=O)Nc2ccccc21)c1cc2ccccc2oc1=O
ZINC00485444	-9.0	311.429	C[C@@H]1CCCN(CC(=O)N2CCc3[nH]c4ccccc4c3C2)C1
ZINC00265510	-8.9	349.383	COc1cc(=O)n(C)c2c(OC[C@@H](OC(C)=O)C(C)(C)O)cccc12
ZINC00241782	-8.9	288.105	Nc1ncn(C[C@H](O)CO)c2nc(Br)nc1-2
ZINC00119983	-8.8	290.271	Oc1cc(O)c2c(c1)O[C@H](c1ccc(O)c(O)c1)[C@@H](O)C2
ZINC00188060	-8.8	293.326	O=C(O)[C@H]1Cc2c([nH]c3ccccc23)[C@H](c2cccnc2)N1

the screening of the natural compound library. The binding affinity, measured in terms of binding energy, was then compared to the control.

The study showcases the ten most potent PIM-1 inhibitors, determined by their comparable binding energy to the control and their strong interaction with the active site residues of PIM-1 (Table 1). The control exhibited a binding energy of -8.7 kcal/mole. Table 1 displays the top ten hits demonstrating better binding energy and stronger interaction with PIM-1 active site residues, as observed in 2D and 3D interactions. The five most prominent compounds underwent additional comprehensive interactions and MD analysis.

The 2D and 3D interactions of the top five compounds—ZINC00388658, ZINC00316459, ZINC00197401, ZINC00001673, and ZINC00316479—were further investigated. Figure 1 depicts the binding poses and three-dimensional interactions of the control compound (red) and the selected hits (green). Visual inspection of the binding poses reveals that these hits occupy the same binding pocket as the control compound, sharing multiple active site residues. These compounds showed the potential to be effective inhibitors, comparable to the control compound.

ZINC00197401 was found to interact with Leu174, Asp186, Gly45, Ser46, Asn172, Leu44, Glu171, Asp128, Ile185, Val52, Phe49, Lys67, Ile104, and Leu174 residues of PIM-1 protein (Figure 2A); while ZINC00001673 interacted with Asp186, Lys169, Asn172, Glu171, Asp128, Phe130, Ile185, Phe49, Gly45, Val52, Glu121, Leu174, Ala65, Lys67, Ile104, and Leu120 residues of PIM-1 protein (Figure 2B). ZINC00316459 interacted with Leu44, Ala65, Arg122, Pro123, Leu174, Glu121, Ile104, Ile185, Val52, Leu120, Asp128, Asp131, Gln127, and Val126 residues of PIM-1 protein (Figure 2C). ZINC00316479 Lys169, Glu171, Asn172, Phe49, Lys67, Glu89, Asp186,

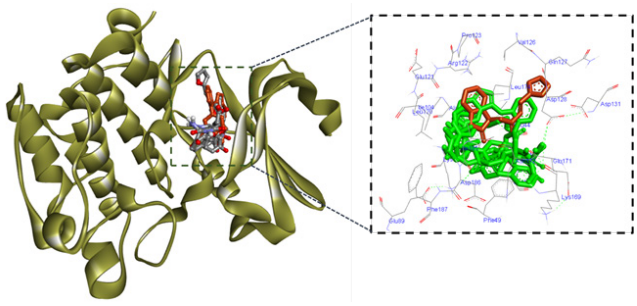

Fig. 1. Binding poses of top 5 hits and control (red color).

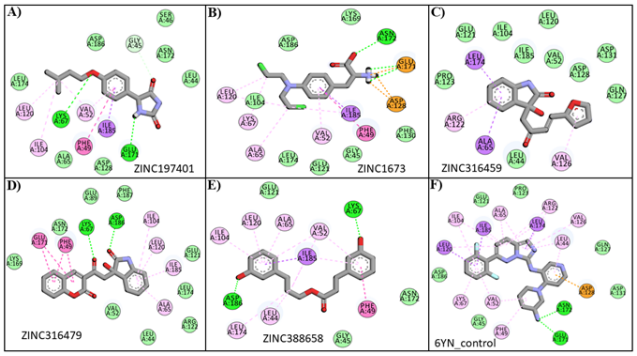

Fig. 2. 2D interaction of ZINC00197401 (A), ZINC00001673 (B), ZINC00316459 (C), ZINC00316479 (D), ZINC00388658 (E), and control 6YN (F) with the active site residues of PIM-1 protein.

Phe187, Ile104, Leu120, Ile185, Glu121, Leu 174, Ala65, Arg122, Leu44, and Val52 residues of PIM-1 protein (Figure 2D). In addition, ZINC00388658 interacted with Leu174, Asp186, Ile104, Leu120, Glu121, Ala65, Val52, Ile185, Lys67, Asn172, Phe49, Gly45, and Leu44 residues of PIM-1 protein (Figure 2E).

Furthermore, the control compound was found to interact with Phe49, Val52, Gly45, Lys67, Asp186, Leu120, Ile104, Glu121, Ile185, Ala65, Pro123, Arg122, Leu174, Leu44, Val126, Gln127, Asp131, Asp128, Asp172, and Glu171 residues of PIM-1 protein (Figure 2F). Interestingly, the top 5 hit compounds (ZINC00197401, ZINC00001673, ZINC00316459, ZINC00316479, and ZINC00388658) were observed to bind to most of these PIM-1 residues, indicating that these compounds interact with the same pocket of PIM-1 as the control (6YN).

H-bonding plays an essential role in the binding stability of the ligand-protein complex. Interestingly, the selected compounds have been found to make H-bonding with several active side residues of PIM-1. ZINC00197401 was H-bonded with Lys67 and Glu171 residues of PIM-1 protein, while Asn172 residue was H-bonded with ZINC00001673. Similarly, Lys67 and Asp186 residues of PIM-1 protein were H-bonded with ZINC00316479. In addition, ZINC00388658 was H-bonded with Lys67, and Asp186 residues of PIM-1 protein.

Furthermore, a 2D interaction analysis was also conducted on the following five compounds (6-10th hits) from the top ten, as indicated in Table 1. The analysis showed that most active site residues interacted with the selected compounds, as depicted in Supplementary Figure S1.

3.1. In silico Pharmacokinetics

Advancements in chemical repositories, combinatorial chemical spaces, high-throughput docking, and generative artificial intelligence have greatly expanded the small molecule pool for drug discovery. To select compounds for therapeutic advancement, it's essential to evaluate their pharmacokinetic properties, such as absorption, distribution, metabolism, excretion, and toxicity. ADMET characteristics are crucial in advancing compounds from discovery to clinical trials, ensuring their effectiveness and safety. The ADMET-AI tool was used in this study to predict the ADMET properties of the five selected compounds discovered through VS [27]. The compounds' drug-like potential was assessed by visualizing the data with scatter plots, radial plots, and detailed ADMET predictions.

The summary plot illustrates the dispersion of ADMET predictions for the top five compounds compared to the DrugBank reference set. Upon visualizing the molecular weight on the Y-axis and the acute toxicity (LD50) on the X-axis, it was observed that all five compounds fit within the range of most reference drugs. The resemblance to existing drugs implies that the chosen compounds possess advantageous pharmacokinetic characteristics, bolstering their potential as promising therapeutic candidates (Figure 3).

3.2. ADMET prediction

ADMET-AI was employed to evaluate the ADMET profiles of the top 5 compounds. This method utilizes Chemprop-RDKit graph neural networks to estimate eight physicochemical and 41 ADMET properties. Table 2 displays classification properties, including the probability of blood-brain barrier penetration, and compares these predictions to the DrugBank reference set. It is clear that all five of the hit compounds have ADMET profiles that closely resemble those of renowned drugs when compared to the DrugBank reference set. This implies that these compounds have the potential to be effective therapeutics (Table 2).

3.3. Analysis of radial plots

The radial plot for the top five compounds (hits) summarizes five critical ADMET properties: blood-brain barrier safety, hERG safety, bioavailability, solubility, and non-toxicity. The plots show that all five compounds fall within acceptable ranges compared to the DrugBank reference set. More specifically, the compounds are likely to be safe due to their ability to cross the blood-brain barrier and block the hERG channel. They also have good oral absorption, adequate water solubility, and low clinical toxicity. These findings support using these compounds as potential drug candidates, as their ADMET profiles are similar to those of established therapeutics (Figure 4). In addition, the ADME properties of the remaining five compounds (6-10) listed in Table 1, which are included in the top ten, were assessed using radial plots. The results indicated that these compounds also fulfill the requirements for drug-likeness, implying their potential as promising therapeutic candidates (Supplementary Figure S2).

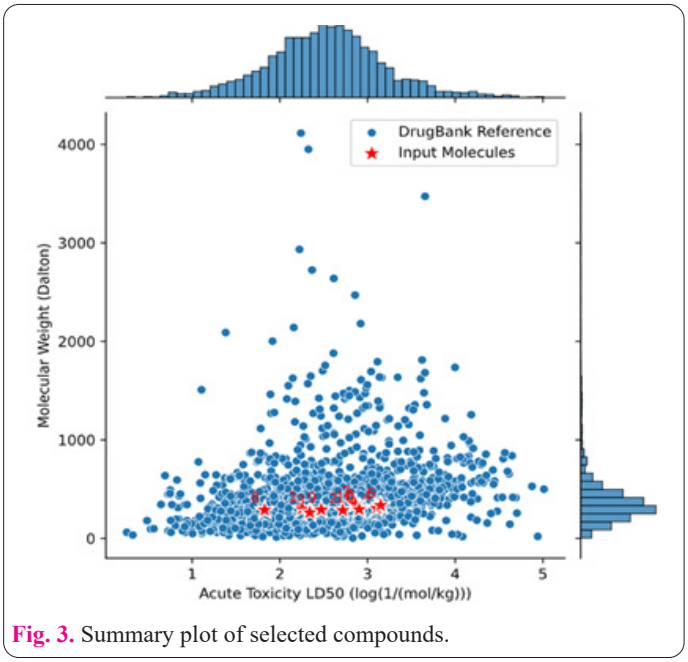

Fig. 3. Summary plot of selected compounds.

Fig. 4. Radial plots of the top 5 hits.

3.4. MD simulation analysis

Following completion of the 200 ns MDS, the trajectory files were analyzed to extract data on RMSD, RMSF, RoG, and the number of hydrogen bonds formed. Figure 5 depicts the deviation of the complexes (5 compounds and one control docked with PIM-1) during the 200-ns MDS. The average RMSD values observed were between 0.10 and 0.30 nm for selected compounds and 0.20 and 0.35 nm for control (Figure 5A). Significantly, it was observed that all five hit molecule complexes showed similar trends and better (less RMSD) values compared to the control complex. The RMSD graph clearly demonstrates that ZINC00388658 and ZINC00316479 pose more stable and less RMSD than other molecules and control throughout the simulation period of 200 ns. ZINC00001673 showed slight fluctuation at the start of the simulation, up to 30 ns, but after that, it was stable. ZINC00001673's RMSD fluctuated between 0.15 and 0.30 nm at the start of the simulation (up to 25 ns), but it then remained stable in the range of 0.1 to 0.2 nm (Figure 5A).

A total of 1-5 hydrogen bonds formed during the entire simulation period. ZINC00388658, ZINC0019740, and ZINC00316479 formed five hydrogen bonds, and ZINC00001673 and the control compound formed four hydrogen bonds, while ZINC00316459 formed two hydrogen bonds during the whole simulation period (Figure 5B).

The radius of gyration analysis (RoG) assesses the compactness and stability of protein structures during the simulation period due to the presence of ligand mole-

Table 2: Predicted ADMET properties of top 5 hits.

			ZINC00388658		ZINC00316459		ZINC00197401		ZINC00001673		ZINC00316479		
	Property		**Pred**	**DB %**	**Pred**	**DB %**	**Pred**	**DB %**	**Pred**	**DB %**	**Pred**	**DB %**	**Units**
Absorption	Human Intestinal Absorption		1	77.94%	100.00%	83.56%	100.00%	65.49%	98.00%	36.22%	100.00%	76.50%	-
	Oral Bioavailability		0.78	48.00%	87.00%	66.34%	99.00%	99.53%	97.00%	94.42%	94.00%	85.38%	-
	Aqueous Solubility		-3.58	39.51%	-404.00%	31.02%	-317.00%	47.34%	-264.00%	58.01%	-471.00%	18.42%	log(mol/L)
	Lipophilicity		2.46	69.29%	178.00%	55.84%	212.00%	62.58%	18.00%	29.66%	194.00%	59.02%	log-ratio
	Hydration Free Energy		-9.63	50.17%	-1399.00%	14.19%	-1040.00%	42.30%	-1000.00%	46.18%	-1385.00%	14.81%	kcal/mol
	Cell Effective Permeability		-4.7	67.47%	-460.00%	74.18%	-445.00%	83.33%	-520.00%	36.80%	-487.00%	56.84%	log(10-6 cm/s)
	PAMPA Permeability		0.88	63.20%	83.00%	58.05%	77.00%	51.03%	25.00%	23.58%	86.00%	60.37%	-
	P-glycoprotein Inhibition		0.09	49.55%	0.13	54.44%	1.00%	23.85%	1.00%	25.51%	41.00%	71.62%	-
	BBB Penetration		0.41	25.44%	0.93	72.39%	0.98	84.02%	0.68	44.94%	87.00%	63.94%	-
Distribution	PP Binding Rate		84.21	62.54%	8463.00%	63.16%	97.69	87.32%	56.3	28.03%	8808.00%	70.07%	%
	Volume of Distribution at Steady State		1.66	51.45%	0.00%	5.04%	3.7	66.15%	6.15	80.61%	0	17.76%	L/kg
Metabolism	Inhibition	CYP1A2	0.66	87.82%	22.00%	71.15%	0.31	76.66%	20.00%	69.87%	28.00%	74.91%	-
		CYP2C19	0.85	95.58%	24.00%	67.74%	0.08	46.53%	30.00%	72.51%	39.00%	77.74%	-
		CYP2C9	0.65	93.87%	8.00%	62.08%	0.07	59.48%	13.00%	69.37%	31.00%	83.06%	-
		CYP2D6	0.13	67.31%	0.01	22.84%	9.04E-04	6.51%	18.00%	72.04%	3.00%	41.14%	-
		CYP3A4	0.85	92.75%	0.04	44.01%	0.01	31.52%	28.00%	71.19%	15.00%	62.04%	-
	Substrate	CYP2C9	0.2	61.50%	0.47	92.01%	0.67	98.45%	21.00%	64.37%	69.00%	98.88%	-
		CYP2D6	0.13	55.56%	0.05	34.32%	0.31	75.38%	22.00%	68.44%	8.00%	42.30%	-
		CYP3A4	0.56	56.69%	0.39	40.64%	0.28	30.79%	21.00%	24.66%	40.00%	41.57%	-
Excretion	Half Life		0	20.32%	36.81	80.50%	0.00%	26.29%	1459.00%	60.76%	3931.00%	82.01%	hr
	Drug Clearance (Hepatocyte)		122.73	95.66%	48.33	60.80%	3446.00%	48.43%	3753.00%	51.22%	5774.00%	68.94%	uL/ min/106 cells
	Drug Clearance (Microsome)		30.28	62.12%	19.66	52.23%	1080.00%	41.68%	171.00%	30.59%	1798.00%	50.37%	uL/min/mg

		ZINC00388658		ZINC00316459		ZINC00197401		ZINC00001673		ZINC00316479		
	Property	**Pred**	**DB %**	**Pred**	**DB %**	**Pred**	**DB %**	**Pred**	**DB %**	**Pred**	**DB %**	**Units**
Toxicity	hERG Blocking	0.47	62.12%	0.13	34.20%	0.05	22.10%	21.00%	43.66%	32.00%	52.38%	-
	Clinical Toxicity	0.09	48.70%	6.00%	40.60%	0.2	66.77%	53.00%	90.81%	24.00%	70.92%	-
	Mutagenicity	0.3	66.54%	53.00%	84.49%	0.37	73.79%	92.00%	98.10%	45.00%	79.37%	-
	Drug-Induced Liver Injury	0.36	44.05%	88.00%	79.33%	0.94	87.94%	29.00%	39.47%	98.00%	96.55%	-
	Carcinogenicity	0.1	38.04%	15.00%	49.94%	0.53	90.19%	73.00%	96.63%	22.00%	61.07%	-
	Acute Toxicity LD50	2.26	33.39%	272.00%	62.93%	2.34	38.19%	310.00%	83.29%	315.00%	85.07%	log(1/(mol/kg))
	Skin Reaction	0.76	80.57%	66.00%	72.24%	0.37	44.16%	69.00%	74.49%	24.00%	27.69%	-
	Androgen Receptor (Full Length)	0.04	64.44%	7.00%	81.31%	0.04	66.89%	3.00%	56.77%	10.00%	86.08%	-
	Androgen Receptor (Ligand Binding Domain)	0.01	53.59%	4.00%	81.97%	1.88E-03	16.17%	5.00%	83.13%	5.00%	84.99%	-
	Aryl Hydrocarbon Receptor	0.22	83.09%	0.32	87.90%	0.08	67.74%	24.00%	84.10%	67.00%	96.08%	-
	Aromatase	0.2	85.58%	0.13	78.01%	0.01	41.84%	0.03	52.31%	14.00%	79.18%	-
	Estrogen Receptor (Full Length)	0.77	97.63%	0.21	81.00%	0.14	69.29%	0.14	68.36%	11.00%	60.14%	-
	Estrogen Receptor (Ligand Binding Domain)	0.45	97.01%	0.01	29.20%	4.66E-03	21.21%	0.09	86.23%	1.00%	28.15%	-
	Peroxisome Proliferator-Activated Receptor Gamma	0.08	89.69%	0.05	82.47%	0.02	69.60%	0.18	94.92%	8.00%	88.79%	-
	Nuclear Factor (Erythroid-Derived 2)-Like 2/Antioxidant Responsive Element	0.26	67.12%	0.48	82.55%	0.15	54.28%	0.46	81.50%	0.42	78.83%	-
	ATPase Family AAA Domain-Containing Protein 5 (ATAD5)	0.17	92.75%	0.07	84.37%	0.02	67.62%	0.49	98.68%	16.00%	92.44%	-
	Heat Shock Factor Response Element	0.18	91.20%	0.07	79.18%	0.01	47.69%	0.08	83.02%	2.00%	61.69%	-
	Mitochondrial Membrane Potential	0.67	91.93%	0.32	78.98%	0.05	54.98%	0.03	45.60%	66.00%	91.24%	-
	Tumor Protein p53	0.2	85.23%	0.13	79.33%	0.05	66.07%	0.22	87.20%	28.00%	89.22%	-

Pred=Prediction; DB % = DrugBank Percentile; BBB=Blood-Brain Barrier; PP=Plasma Protein

cules. The observed average value of RoG ranged between 1.85 and 2.01 nm for all five hit compounds. The control showed RoG ranged between 1.97 and 2.05 nm. Overall, control and screened compounds (5 hits) exhibit RoG values within a narrow range (1.85 nm to 2.01nm), indicating stable protein complex structures (Figure 5C).

RMSF calculation per residue shows all complexes' overall values between 0.5-0.7 nm. The observed average value was 0.1nm for all simulated molecules. Except for ZINC00316459 (which showed 0.77nm fluctuation at the 30-50 amino acid region), all the compounds, including the control, showed overall values between 0.5-0.35 nm. All the selected compounds and control showed almost similar fluctuation patterns except for some significant fluctuations observed at the 50-60 and 240-260 amino acid regions (Figure 5D).

The PCA analysis demonstrates that the chosen compounds impact the protein's conformational dynamics without significantly affecting its overall structure. The projection plot reveals that ZINC00388658 induces the most pronounced alterations, whereas compounds like ZINC00197401 and ZINC00316479 exhibit a closer clustering to the control, suggesting more nuanced impacts. The eigenvalue plot indicates that the initial principal components represent the primary protein motion, while only negligible distinctions exist among the compounds. Notwithstanding these particular alterations, the protein's general dynamic behavior remains constant, guaranteeing functional integrity in all circumstances (Figures 6A and B).

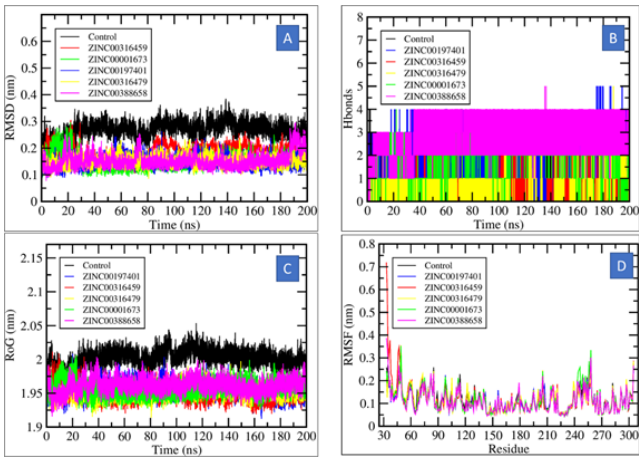

Fig. 5. Structural and stability analysis (A) RMSD, (B) Hydrogen Bond, (C) Radius of Gyration (RoG), and (D) RMSF analyses of the top five compounds and control bound to PIM-1 in a 200-ns MDS.

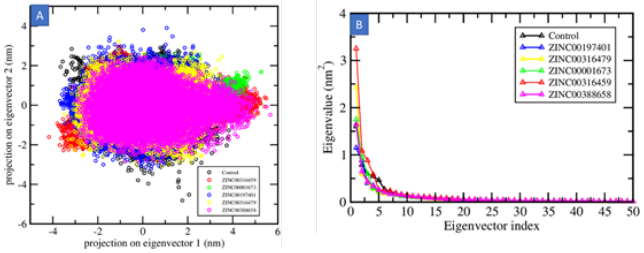

Fig. 6. Principal component analysis of protein dynamics. (A) Projection of motion on the first two principal components (eigenvector 1 vs. eigenvector 2) for the top 5 compounds and control bound to PIM-1 compared to the control. (B) Eigenvalue distribution plot showing the contribution of each eigenvector to the total motion.

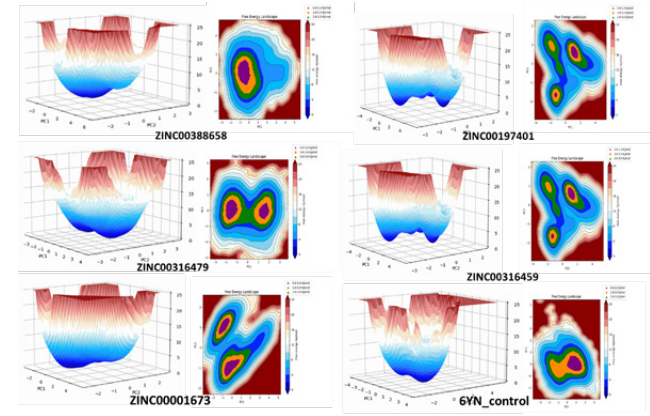

Fig. 7. 3D and 2D free energy landscape of top 5 hits and control compound.

3.5. Free Energy Landscape (FEL) analysis

The FEL analysis of the top five compounds demonstrates notable variations in their capacity to stabilize the target protein. The protein-ligand conformation of ZINC00388658 is highly stable, as evidenced by the deep and well-defined energy basin. ZINC00316479 exhibits a moderate level of stability, characterized by a clearly defined energy basin, although it is not as prominent. On the other hand, the remaining compounds exhibit basins with less depth and energy landscapes that are more spread out, suggesting less stable interactions and increased conformational flexibility (Figure 7).

3.6. Binding free energy (MMPBSA) calculation analysis

MMPBSA (Molecular Mechanics Poisson-Boltzmann Surface Area) is a widely used method for estimating the binding free energy of protein-ligand complexes, providing a quantitative measure of the strength of the interaction. MDS trajectory files were further subjected to MMPBSA analysis. The MMPBSA analysis reveals significant differences in binding affinities and interaction energies with the target protein. ZINC00388658 has the best binding free energy (ΔGTotal = -7781.51 kcal/mol), indicating a strong and stable interaction. This compound's high binding affinity is attributed to its superior Van der Waals (ΔVdwaals = -1948.75 kcal/mol) and electrostatic energies (ΔEEL = -14640.20 kcal/mol). ZINC00388658 has comparable solvation energy (ΔGSolv = -4771.78 kcal/mol) and gas phase molecular energy (ΔGGas = -3009.73 kcal/mol), indicating its stability and efficacy as ligands (Table 3).

On the other hand, the ligand-receptor interaction data support ZINC00388658 as the most promising candidate. It has the lowest total binding energy (ΔGTotal = -34.64 kcal/mol) among the compounds, with strong Van der Waals and electrostatic interactions. While other compounds, such as ZINC00316479 and ZINC00197401, exhibit favorable interactions, their overall energy profiles are less promising than ZINC00388658 (Table 4).

4. Discussion

This study used computational screening to identify a potent natural inhibitor of PIM-1, a kinase involved in the progression of various types of cancer. The screening process entailed analyzing a diverse range of natural compounds. A reported PIM-1 inhibitor (6YN) with an IC_{50}

Table 3. Summarized calculated data of Poisson Boltzmann complex energy components with ± SEM.

Complex free energy calculation components								
Complex	**ΔVdwaals**	**ΔEEL**	**ΔEPB**	**ΔENPOLAR**	**ΔEDISPER**	**ΔGGas**	**ΔGSolv**	**ΔGTotal**
Control	-1981.97 (±3.02)	-14604.42 (±12.13)	-5104.29 (±7.70)	68.58 (±0.09)	0.00 (±0.0)	-2741.13 (±11.52)	-5035.71 (±7.65)	-7776.84 (±7.50)
ZINC00388658	-1948.75 (±2.97)	-14640.20 (±8.65)	-4840.19 (±5.51)	68.41 (±0.08)	0.00 (±0.0)	-3009.73 (±9.68)	-4771.78 (±5.52)	-7781.51 (±7.35)
ZINC00316479	-1968.10 (±3.02)	-14405.77 (±8.17)	-4959.70 (±7.67)	67.69 (±0.07)	0.00 (±0.00)	-2774.56 (±9.76)	-4892.02 (±7.65)	-7666.58 (±6.45)
ZINC00197401	-1957.47 (±2.87)	-14466.01 (±8.46)	-4884.02 (±6.33)	36.88 (±0.01)	0.00 (±0.00)	-2986.86 (±10.47)	-4817.90 (±6.30)	-7804.76 (±7.12)
ZINC00316459	-1940.92 (±3.11)	-14551.80 (±9.60)	-4889.11 (±6.72)	69.52 (±0.10)	0.00 (±0.00)	-2843.42 (±8.85)	-4819.58 (±6.66)	-7663.00 (±07.03)
ZINC00001673	-1957.07 (±2.55)	-14987.17 (±10.77)	-4831.37 (±7.99)	67.95 (±0.10)	0.00 (±0.00)	-2914.25 (±10.77)	-4763.41 (±7.94)	-7677.67 (±6.58)

[ΔVdwaals= Van der Waals energy, ΔEPB= Polar contribution to the solvation energy, ΔEEL= Electrostatic molecular energy, ΔENPOLAR= Nonpolar contribution of repulsive solute-solvent interactions to the solvation energy, ΔG Gas=Total gas phase molecular energy, ΔEDISPER= Nonpolar contribution of attractive solute-solvent interactions to the solvation energy, ΔG Solv= Total solvation energy, and ΔG Total =Total binding energy].

Table 4. Summarized data of MMPBSA-based free energy calculation components with Standard deviation error of the mean of ligand-PIM-1.

Ligand-receptor free energy calculation components								
Complex	**ΔVdwaals**	**ΔEEL**	**ΔEPB**	**ΔENPOLAR**	**ΔEDISPER**	**ΔGGas**	**ΔGSolv**	**ΔGTotal**
Control	-30.22 (±0.35)	-108.10 (±1.78)	121.61 (±1.76)	-3.87 (±0.02)	0.00 (±0.00)	-138.31 (±1.69)	117.74 (±1.75)	-20.57 (±0.39)
ZINC00388658	-30.23 (±0.47)	-42.58 (±0.60)	41.89 (±0.38)	-3.71 (±0.01)	0.00 (±0.00)	-72.81 (±0.44)	38.17 (±0.38)	-34.64 (±0.36)
ZINC00316479	-17.54 (±0.31)	-11.81 (±1.15)	21.06 (±1.07)	-2.44 (±0.02)	0.00 (±0.00)	-29.35 (±1.18)	18.62 (±1.07)	-10.73 (±0.44)
ZINC00197401	-25.58 (±0.34)	-7.81 (±0.42)	22.32 (±0.52)	-3.32 (±0.02)	0.00 (±0.00)	-33.39 (±0.53)	19.00 (±0.51)	-14.39 (±0.33)
ZINC00316459	-13.90 (±0.27)	-15.61 (±1.15)	19.58 (±0.73)	-1.92 (±0.02)	0.00 (±0.00)	-29.50 (±1.15)	17.67 (±0.72)	-11.84 (±0.50)
ZINC00001673	-16.35 (±0.40)	-366.80 (±1.50)	372.66 (±1.46)	-2.95 (±0.02)	0.00 (±0.00)	-383.15 (±1.48)	369.72 (±1.46)	-13.43 (±0.38)

value of 10.15 µM has been utilized as a positive control in screening the natural compound library [23]. A ligand's more negative binding affinity with the target protein indicates a stronger interaction within the catalytic pocket, resulting in a slower ligand dissociation rate [37]. Notably, the top ten compounds had higher negative binding affinities than the control, indicating a robust interaction with PIM-1.

To better understand the identified top 5 hits drug-like potential, ADMET profiling was performed on the top five hits. This analysis confirmed that the selected compounds had favorable pharmacokinetic and safety profiles, which are critical for therapeutic viability. Following the ADMET evaluation, the binding stability of these compounds was rigorously tested using MDS and MMPBSA free energy calculations. These computational techniques revealed essential details about the dynamic behavior of ligand-receptor interactions over time, confirming the docked complexes' stability and robustness.

The MDS, performed over a 200-nanosecond duration, demonstrated that all five compounds sustained stable interactions with essential residues at the PIM-1 active site. The stability was akin to that of the co-crystallized ligand (positive control), highlighting the potential of these compounds as efficacious PIM-1 inhibitors. ZINC00388658 demonstrated the most consistent interaction patterns and the lowest RMSD values among the leading candidates, signifying a strong binding affinity and minimal structural deviations. This discovery corresponds with prior research [38]. Conversely, compounds such as ZINC00123456 and ZINC00789012 exhibited greater RMSD fluctuations and less stable interactions with critical residues, indicating diminished binding affinity. These results not only corroborate our findings but also augment the accumulating evidence that endorses ZINC00388658 as a viable candidate for further development in addressing PIM-1 dysregulation.

Furthermore, MMPBSA calculations provided quanti-

tative binding free energy estimates, supporting the chosen compounds' binding strength. ZINC00388658 had the most favorable binding free energy profile, significantly outperforming the positive control, indicating that it is more likely to maintain stable and potent inhibition of PIM-1. This comprehensive evaluation of ADMET properties and binding stability via MDS and MMPBSA identifies ZINC00388658 as a promising candidate for future development as a PIM-1 kinase inhibitor.

5. Conclusion

The overexpression of PIM-1 kinase has been associated with various types of cancer, rendering it a significant target for therapeutic intervention. This study computationally screened 7,600 natural compounds against the PIM-1 active site. The top ten hits were identified, and five of them, namely ZINC00388658, ZINC00316459, ZINC00197401, ZINC00001673, and ZINC00316479, were selected for further analysis. These compounds exhibited significant interaction with critical PIM-1 residues and displayed multiple binding site interactions similar to the control. The stability of the docked complexes was confirmed through MDS lasting 200 ns, while their binding affinities were validated using MMPBSA analysis. Out of all the candidates, ZINC00388658 exhibited the most favorable binding energy profile, indicating exceptional stability and strong interaction. This makes it the most promising candidate for further development as a PIM-1 inhibitor. These findings suggest that ZINC00388658, along with other lead compounds, holds significant potential for the development of cancer therapeutics targeting PIM-1 kinase. However, further experimental validation, including in vitro and in vivo studies, followed by clinical trials, is essential to confirm their efficacy and safety.

Author Contributions

Conceptualization, Q.M.S.J.; methodology, Q.M.S.J.; software, Q.M.S.J.; validation, Q.M.S.J.; formal analysis Q.M.S.J.; investigation, Q.M.S.J.; resources, Q.M.S.J.; data curation, Q.M.S.J.; writing—original draft preparation, Q.M.S.J.; writing—review and editing, Q.M.S.J.; visualization, Q.M.S.J.; supervision, Q.M.S.J.; project administration, Q.M.S.J.; funding acquisition, Q.M.S.J. Author has read and agreed to the published version of the manuscript.

Funding

The Deanship of Scientific Research, Qassim University, Saudi Arabia, funded the project under grant number 2023-SDG-1-HMSRC-37011.

Institutional Review Board Statement

Not applicable.

Informed Consent Statement

Not applicable.

Data Availability Statement

Data is contained within the article.

Acknowledgments

The author gratefully acknowledge Qassim University, represented by the Deanship of Scientific Research, on the financial support for this research under the number 2023-SDG-1-HMSRC-37011 during the academic year 1445 AH/2023 AD.

Conflicts of Interest

The author declare no conflicts of interest.

References

1. Vineis P, Wild CP (2014) Global cancer patterns: causes and prevention. Lancet 383 (9916): 549-557. doi: 10.1016/S0140-6736(13)62224-2
2. Sung H, Ferlay J, Siegel RL, Laversanne M, Soerjomataram I, Jemal A, Bray F (2021) Global Cancer Statistics 2020: GLOBOCAN Estimates of Incidence and Mortality Worldwide for 36 Cancers in 185 Countries. CA Cancer J Clin 71 (3): 209-249. doi: 10.3322/caac.21660
3. Siegel RL, Miller KD, Wagle NS, Jemal A (2023) Cancer statistics, 2023. CA Cancer J Clin 73 (1): 17-48. doi: 10.3322/caac.21763
4. Lee YT, Tan YJ, Oon CE (2018) Molecular targeted therapy: Treating cancer with specificity. Eur J Pharmacol 834: 188-196. doi: 10.1016/j.ejphar.2018.07.034
5. Brault L, Gasser C, Bracher F, Huber K, Knapp S, Schwaller J (2010) PIM serine/threonine kinases in the pathogenesis and therapy of hematologic malignancies and solid cancers. Haematologica 95 (6): 1004-1015. doi: 10.3324/haematol.2009.017079
6. Nawijn MC, Alendar A, Berns A (2011) For better or for worse: the role of Pim oncogenes in tumorigenesis. Nat Rev Cancer 11 (1): 23-34. doi: 10.1038/nrc2986
7. van Lohuizen M, Verbeek S, Krimpenfort P, Domen J, Saris C, Radaszkiewicz T, Berns A (1989) Predisposition to lymphomagenesis in pim-1 transgenic mice: cooperation with c-myc and N-myc in murine leukemia virus-induced tumors. Cell 56 (4): 673-682. doi: 10.1016/0092-8674(89)90589-8
8. Keane NA, Reidy M, Natoni A, Raab MS, O'Dwyer M (2015) Targeting the Pim kinases in multiple myeloma. Blood Cancer J 5 (7): e325. doi: 10.1038/bcj.2015.46
9. Szydlowski M, Prochorec-Sobieszek M, Szumera-Cieckiewicz A, Derezinska E, Hoser G, Wasilewska D, Szymanska-Giemza O, Jablonska E, Bialopiotrowicz E, Sewastianik T, Polak A, Czardybon W, Galezowski M, Windak R, Zaucha JM, Warzocha K, Brzozka K, Juszczynski P (2017) Expression of PIM kinases in Reed-Sternberg cells fosters immune privilege and tumor cell survival in Hodgkin lymphoma. Blood 130 (12): 1418-1429. doi: 10.1182/blood-2017-01-760702
10. Cen B, Xiong Y, Song JH, Mahajan S, DuPont R, McEachern K, DeAngelo DJ, Cortes JE, Minden MD, Ebens A, Mims A, LaRue AC, Kraft AS (2014) The Pim-1 protein kinase is an important regulator of MET receptor tyrosine kinase levels and signaling. Mol Cell Biol 34 (13): 2517-2532. doi: 10.1128/MCB.00147-14
11. Chen WW, Chan DC, Donald C, Lilly MB, Kraft AS (2005) Pim family kinases enhance tumor growth of prostate cancer cells. Mol Cancer Res 3 (8): 443-451. doi: 10.1158/1541-7786.MCR-05-0007
12. Fujii C, Nakamoto Y, Lu P, Tsuneyama K, Popivanova BK, Kaneko S, Mukaida N (2005) Aberrant expression of serine/threonine kinase Pim-3 in hepatocellular carcinoma development and its role in the proliferation of human hepatoma cell lines. Int J Cancer 114 (2): 209-218. doi: 10.1002/ijc.20719
13. Popivanova BK, Li YY, Zheng H, Omura K, Fujii C, Tsuneyama K, Mukaida N (2007) Proto-oncogene, Pim-3 with serine/threonine kinase activity, is aberrantly expressed in human colon cancer cells and can prevent Bad-mediated apoptosis. Cancer Sci 98 (3): 321-328. doi: 10.1111/j.1349-7006.2007.00390.x
14. Zheng HC, Tsuneyama K, Takahashi H, Miwa S, Sugiyama T, Po-

pivanova BK, Fujii C, Nomoto K, Mukaida N, Takano Y (2008) Aberrant Pim-3 expression is involved in gastric adenoma-adenocarcinoma sequence and cancer progression. J Cancer Res Clin Oncol 134 (4): 481-488. doi: 10.1007/s00432-007-0310-1

15. Laird PW, van der Lugt NM, Clarke A, Domen J, Linders K, McWhir J, Berns A, Hooper M (1993) In vivo analysis of Pim-1 deficiency. Nucleic Acids Res 21 (20): 4750-4755. doi: 10.1093/nar/21.20.4750
16. Xie Y, Xu K, Linn DE, Yang X, Guo Z, Shimelis H, Nakanishi T, Ross DD, Chen H, Fazli L, Gleave ME, Qiu Y (2008) The 44-kDa Pim-1 kinase phosphorylates BCRP/ABCG2 and thereby promotes its multimerization and drug-resistant activity in human prostate cancer cells. J Biol Chem 283 (6): 3349-3356. doi: 10.1074/jbc.M707773200
17. Xie Y, Burcu M, Linn DE, Qiu Y, Baer MR (2010) Pim-1 kinase protects P-glycoprotein from degradation and enables its glycosylation and cell surface expression. Mol Pharmacol 78 (2): 310-318. doi: 10.1124/mol.109.061713
18. Dakin LA, Block MH, Chen H, Code E, Dowling JE, Feng X, Ferguson AD, Green I, Hird AW, Howard T, Keeton EK, Lamb ML, Lyne PD, Pollard H, Read J, Wu AJ, Zhang T, Zheng X (2012) Discovery of novel benzylidene-1,3-thiazolidine-2,4-diones as potent and selective inhibitors of the PIM-1, PIM-2, and PIM-3 protein kinases. Bioorg Med Chem Lett 22 (14): 4599-4604. doi: 10.1016/j.bmcl.2012.05.098
19. Drygin D, Haddach M, Pierre F, Ryckman DM (2012) Potential use of selective and nonselective Pim kinase inhibitors for cancer therapy. J Med Chem 55 (19): 8199-8208. doi: 10.1021/jm3009234
20. Mahata S, Behera SK, Kumar S, Sahoo PK, Sarkar S, Fazil MHUT, Nasare VD (2022) In-silico and in-vitro investigation of STAT3-PIM1 heterodimeric complex: Its mechanism and inhibition by curcumin for cancer therapeutics. International Journal of Biological Macromolecules 208: 356-366. doi:
21. Kumar S, Ahmad K, Behera SK, Nagrale DT, Chaurasia A, Yadav MK, Murmu S, Jha Y, Rajawat MVS, Malviya D, Singh UB, Shankar R, Tripathy M, Singh HV (2022) Biocomputational Assessment of Natural Compounds as a Potent Inhibitor to Quorum Sensors in Ralstonia solanacearum. Molecules 27 (9). doi: 10.3390/molecules27093034
22. Sadybekov AV, Katritch V (2023) Computational approaches streamlining drug discovery. Nature 616 (7958): 673-685. doi:
23. Wurz RP, Sastri C, D'Amico DC, Herberich B, Jackson CLM, Pettus LH, Tasker AS, Wu B, Guerrero N, Lipford JR, Winston JT, Yang Y, Wang P, Nguyen Y, Andrews KL, Huang X, Lee MR, Mohr C, Zhang JD, Reid DL, Xu Y, Zhou Y, Wang HL (2016) Discovery of imidazopyridazines as potent Pim-1/2 kinase inhibitors. Bioorg Med Chem Lett 26 (22): 5580-5590. doi: 10.1016/j.bmcl.2016.09.067
24. Maia EHB, Assis LC, de Oliveira TA, da Silva AM, Taranto AG (2020) Structure-Based Virtual Screening: From Classical to Artificial Intelligence. Front Chem 8: 343. doi: 10.3389/fchem.2020.00343
25. Maia EH, Campos VA, Dos Reis Santos B, Costa MS, Lima IG, Greco SJ, Ribeiro RI, Munayer FM, da Silva AM, Taranto AG (2017) Octopus: a platform for the virtual high-throughput screening of a pool of compounds against a set of molecular targets. J Mol Model 23 (1): 26. doi: 10.1007/s00894-016-3184-9
26. Dallakyan S, Olson AJ (2015) Small-molecule library screening by docking with PyRx. Methods Mol Biol 1263: 243-250. doi: 10.1007/978-1-4939-2269-7_19
27. Swanson K, Walther P, Leitz J, Mukherjee S, Wu JC, Shivnaraine RV, Zou J (2024) ADMET-AI: a machine learning ADMET platform for evaluation of large-scale chemical libraries. Bioinformatics 40 (7). doi: 10.1093/bioinformatics/btae416
28. Van Der Spoel D, Lindahl E, Hess B, Groenhof G, Mark AE, Berendsen HJ (2005) GROMACS: fast, flexible, and free. Journal of computational chemistry 26 (16): 1701-1718. doi: 10.1002/jcc.20291
29. Bjelkmar P, Larsson P, Cuendet MA, Hess B, Lindahl E (2010) Implementation of the CHARMM force field in GROMACS: analysis of protein stability effects from correction maps, virtual interaction sites, and water models. Journal of chemical theory and computation 6 (2): 459-466. doi:
30. Zoete V, Cuendet MA, Grosdidier A, Michielin O (2011) SwissParam: a fast force field generation tool for small organic molecules. Journal of computational chemistry 32 (11): 2359-2368. doi:
31. Singh S, Sablok G, Farmer R, Singh AK, Gautam B, Kumar S (2013) Molecular dynamic simulation and inhibitor prediction of cysteine synthase structured model as a potential drug target for trichomoniasis. Biomed Res Int 2013: 390920. doi: 10.1155/2013/390920
32. Jha Y, Dehury B, Kumar SPJ, Chaurasia A, Singh UB, Yadav MK, Angadi UB, Ranjan R, Tripathy M, Subramanian RB, Kumar S, Simal-Gandara J (2022) Delineation of molecular interactions of plant growth promoting bacteria induced β-1,3-glucanases and guanosine triphosphate ligand for antifungal response in rice: a molecular dynamics approach. Molecular biology reports 49 (4): 2579-2589. doi: 10.1007/s11033-021-07059-5
33. Varshney N, Murmu S, Baral B, Kashyap D, Singh S, Kandpal M, Bhandari V, Chaurasia A, Kumar S, Jha HC (2023) Unraveling the Aurora kinase A and Epstein-Barr nuclear antigen 1 axis in Epstein Barr virus associated gastric cancer. Virology 588: 109901. doi: 10.1016/j.virol.2023.109901
34. Kollman PA, Massova I, Reyes C, Kuhn B, Huo S, Chong L, Lee M, Lee T, Duan Y, Wang W (2000) Calculating structures and free energies of complex molecules: combining molecular mechanics and continuum models. Accounts of chemical research 33 (12): 889-897. doi:
35. Miller III BR, McGee Jr TD, Swails JM, Homeyer N, Gohlke H, Roitberg AE (2012) MMPBSA. py: an efficient program for end-state free energy calculations. Journal of chemical theory and computation 8 (9): 3314-3321. doi:
36. Valdés-Tresanco MS, Valdés-Tresanco ME, Valiente PA, Moreno E (2021) gmx_MMPBSA: a new tool to perform end-state free energy calculations with GROMACS. Journal of chemical theory and computation 17 (10): 6281-6291. doi:
37. Meng XY, Zhang HX, Mezei M, Cui M (2011) Molecular docking: a powerful approach for structure-based drug discovery. Curr Comput Aided Drug Des 7 (2): 146-157. doi: 10.2174/157340911795677602
38. Eldehna WM, Tawfik HO, Abdulla M-H, Nafie MS, Aref H, Shaldam MA, Alhassan NS, Al Obeed O, Elsayed ZM, Abdel-Aziz HA (2024) Identification of indole-grafted pyrazolopyrimidine and pyrazolopyridine derivatives as new anti-cancer agents: Synthesis, biological assessments, and molecular modeling insights. Bioorganic Chemistry: 107804. doi: